



Research on an early warning method for bearing health diagnosis based on EEMD-PCA-ANFIS

Feng Zhou¹ · Yang Wang¹ · Shan Jiang² · Ting Hao³

Received: 19 June 2022 / Accepted: 3 April 2023 / Published online: 21 April 2023
© The Author(s), under exclusive licence to Springer-Verlag GmbH Germany, part of Springer Nature 2023

Abstract

In response to the problems of single signal information and low accuracy of the early warning method for motor bearing health diagnosis, this paper conducts a study on the early warning method for bearing health diagnosis. By performing ensemble empirical modal decomposition (EEMD) on the signal after empirical modal decomposition (EMD) hard threshold noise reduction and then extracting the vibration signal fault characteristic parameters based on the principal components analysis (PCA) algorithm for dimension reduction, an Ensemble Empirical Modal Decomposition-Principal Components Analysis-Adaptive Network-based Fuzzy Inference System-based (EEMD-PCA-ANFIS) bearing fault warning model for vibration signals under defective conditions is established, the vibration signals of different working conditions are selected for diagnosis, and the accuracy of fault identification reaches 93.3%. Subsequently, a bearing failure warning model based on joint analysis of vibration and temperature rise trends was developed for bearing oil deficiency conditions, and the results show that the model can combine the vibration signal and temperature characteristics to complete the accurate judgement of bearing oil deficiency status and achieve the fault diagnosis of bearing defects and oil deficiency status. Compared with the existing methods, the proposed bearing health diagnosis and early warning method based on Ensemble Empirical Modal Decomposition-Principal Components Analysis-Adaptive Network-based Fuzzy Inference System (EEMD-PCA-ANFIS) can diagnose and warn of bearing defects and the state of oil shortages and oil shortages more accurately and lays a foundation for realizing an intelligent fault warning algorithm based on multi-information fusion.

Keywords Motor bearing · Fault warning · Feature extraction · Status diagnosis · Operation monitoring · EEMD-PCA-ANFIS

1 Introduction

Motors are important driving equipment in modern factories and have a huge number of applications in various fields [1]. The fault detection and intelligent diagnosis of motor bearings have always been the focus of research by scholars at home and abroad [2]. The current detection methods have some problems, such as long time consumption, labor consumption, and low intelligence. Therefore, it is of great

significance to carry out research on the health warning diagnosis method of motor bearings to prevent the occurrence of failures for the safe operation of motors.

Existing bearing monitoring systems generally assess the health of bearing life by monitoring temperature, vibration, noise, speed, voltage, current and other information in real time during bearing operation [3]. For example, Chen Jinhai et al. proposed a new intelligent bearing structure with radial grooves on the outer ring of the bearing to monitor the temperature of the inner ring [4], Gopalakrishna GK et al. monitored the vibration signal through MEMS and carried out bearing health diagnosis [5], Chen Y et al. monitored the bearing vibration signal through FBG to predict the bearing service life [6], Tritschler N et al. developed a condition health monitoring system for regular monitoring of the bearing state [7], etc.

At present, the sensor installation methods of bearing monitoring systems are divided into two types. One is to

✉ Ting Hao
haoting311@163.com

¹ College of Electrical Engineering and Automation, Shandong University of Science and Technology, Qingdao, China

² State Grid Shandong Electric Power Company Maintenance Company, Jinan, China

³ College of Economics and Management, Shandong University of Science and Technology, Qingdao 266590, China

disassemble the motor after welding the sensor to the bearing interior. For example, the embedded intelligent sensor developed by Ren Daqian et al. is used for the measurement of bearing temperature, rotational speed, and vibration [8]. Zhang N et al. proposed an embedded film pressure sensor for monitoring water-lubricated bearings to monitor the water-lubricated shaft oil film pressure, film thickness and film stiffness [9]. Brusa E et al. used fiber optic sensors to monitor the thermal state of bearings [10]. The other is the separate installation of the sensor and bearing. For example, Liu Qinghai and Huang Jianqiu proposed a piezoresistive MEMS composite beam temperature sensor [11]. Xie ZJ et al. proposed a noncontact triboelectric bearing sensor to realize the measurement of bearing speed [12].

From the above literature, it can be seen that most of the bearing health diagnosis and early warning methods used in existing bearing monitoring systems are single information source diagnosis, which has the problem of single signal information, while in monitoring systems with multiple sensors installed, there is more equipment redundancy, which cannot truly achieve multi-information fusion health diagnosis of bearing status.

Currently, the early warning method of motor bearing health diagnosis is divided into two steps: bearing fault feature extraction and fault identification. For feature extraction, short-time Fourier transforms [13], wavelet transforms [14] and empirical mode decomposition [15] are widely used. Fault identification mainly involves research on bearing fault diagnosis algorithms. Common algorithms include naive Bayesian networks [16], K-means clustering algorithms [17], support vector machines [18] and neural networks [19].

In the process of signal processing, the short-time Fourier transform has limitations for the analysis of abrupt signals and nonstationary signals and can only be used for the processing and analysis of stationary signals. Wavelet analysis is not self-adaptive, and it is necessary to continuously try to select different wavelet bases to achieve optimal results in practical applications. EEMD is an improved method of EMD that solves the phenomenon of modal confusion existing in EMD, and the method is self-adaptive and does not need to choose the basis function, such as wavelet transform. Therefore, EEMD is selected as the fault feature extraction method in this paper. For the bearing fault diagnosis algorithm, since ANFIS is an adaptive search algorithm, this method combines the interplay of a neural network and a fuzzy inference system, which is a reliable and effective classification and identification method with better performance than a neural network or fuzzy inference system alone. Therefore, ANFIS is adopted as the bearing fault diagnosis algorithm in this paper.

In summary, most of the existing early warning methods for bearing health diagnosis cannot realize the multi-information fusion health diagnosis of bearing status, and

EEMD and ANFIS have more advantages in bearing fault feature extraction and identification compared with other methods. Therefore, this paper proposes a joint early warning model based on the EEMD-PCA-ANFIS vibration analysis model and bearing temperature rise trend by analyzing bearing fault characteristic parameters to achieve fault diagnosis and oil deficiency state discrimination in the defective state of motor bearings and to provide early warning when a fault occurs or a precursor of fault appears.

2 Motor bearing fault signal processing method

2.1 Motor bearing fault analysis

2.1.1 Classification and manifestation of motor bearing faults

The main causes of motor bearing faults include rotor imbalance, debris in the rotor, friction between dynamic and static parts, bearing corrosion, bearing wear or caps loosening, misalignment of the rotary, low lubricating oil temperature, debris in the lubricating oil or insufficient lubrication, anchor bolt looseness, surge, etc. [20, 21]. Common types of faults in rolling bearings include bearing fatigue, wear, corrosion, indentation, scuffing, cracks, etc. [22]. From the abovementioned various bearing failure mechanisms and manifestations, the abnormal condition of the bearing eventually manifested as vibration, temperature rise, noise and other changes in several aspects [23], and different faults in the same parameters will also reflect different characteristics, of which noise is mainly caused by vibration.

2.1.2 Vibration and temperature characteristic analysis of motor bearing faults

Bearing also produces vibration under normal working conditions, but it is generally caused by its own structural characteristics and the vibration influence of other parts in the motor, and the time-domain vibration waveform is often irregular vibration, without an obvious impact peak and high frequency change. Once a bearing has local defects or faults, the vibration waveform will change significantly.

Under normal circumstances, after the motor has been manufactured, the temperature rise during normal operation does not basically change abruptly or increase continuously with the operation of the motor. However, when the motor is in a fault condition, the motor temperature and the bearing temperature can rise rapidly to the point of burning out the motor. Common damage to rolling bearings generally develops over a long period of time, and their operating temperature rises gradually as the degree of damage increases,

so they can be monitored as indicators of abnormal bearing operating conditions.

In summary, bearings can cause changes in a variety of operating parameters during fault operation, especially vibration and temperature signals, which contain a wealth of information about the characteristics of the fault and can be used to monitor the operating condition of the bearing.

2.2 Bearing vibration and temperature rise signal characteristic analysis and processing method

2.2.1 Bearing vibration signal characteristic analysis and processing method

The undecomposed time-domain signal does not visually reflect the current operating state of the bearing, and traditional signal processing methods such as STFT, Wigner-Ville or wavelet variation methods suffer from poor adaptability and computational complexity. EEMD can decompose complex signals into several intrinsic mode functions (IMFs) [24, 25] based on the signal properties, which is self-adaptive and can solve the phenomenon of mode aliasing existing in EMD and improve the accuracy of signal processing. Therefore, EEMD can be used for feature analysis and processing of bearing vibration signals.

The principle of EEMD decomposition is as follows:

A set of random white noise signals $\{n_1(t), n_2(t), \dots, n_m(t)\}$ with zero mean and equal variance are added to the original signal $x_0(t)$ to obtain a new set of signals $\{x_1(t), x_2(t), \dots, x_m(t)\}$.

$$\begin{cases} x_1(t) = x_0(t) + n_1(t) \\ x_2(t) = x_0(t) + n_2(t) \\ \vdots \\ x_m(t) = x_0(t) + n_m(t) \end{cases} \quad (1)$$

The EMD decomposition of each signal $x_i(t)$ yields m groups of IMFs $\{[C_{11}, C_{12}, \dots, C_{1n}], [C_{21}, C_{22}, \dots, C_{2n}], \dots, [C_{m1}, C_{m2}, \dots, C_{mn}]\}$ (denoted as \mathbf{C}) and m groups of residuals $\{\text{Res}_1, \text{Res}_2, \dots, \text{Res}_m\}$ (denoted as \mathbf{Res}).

$$\mathbf{C} = \begin{bmatrix} C_{11} & C_{12} & \dots & C_{1n} \\ C_{21} & C_{22} & \dots & C_{2n} \\ \vdots & \vdots & \ddots & \vdots \\ C_{m1} & C_{m2} & \dots & C_{mn} \end{bmatrix} \quad \mathbf{Res} = \begin{bmatrix} \text{Res}_1 \\ \text{Res}_2 \\ \vdots \\ \text{Res}_m \end{bmatrix} \quad (2)$$

The mean values corresponding to the m groups of IMFs $\{C_1, C_2, \dots, C_n\}$ and their residuals Res were calculated.

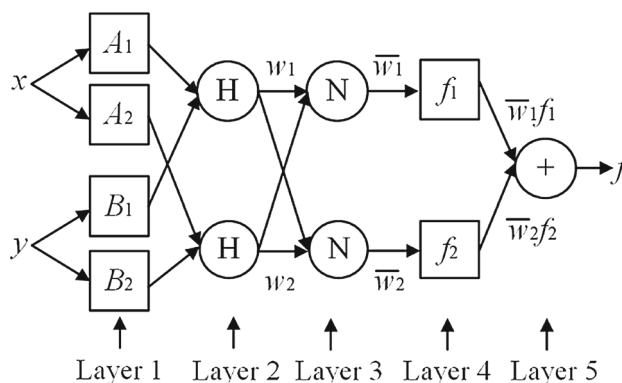


Fig. 1 ANFIS structure diagram

$$\begin{cases} C_1 = \frac{1}{m} \sum_{i=1}^m c_{i1} \\ C_2 = \frac{1}{m} \sum_{i=1}^m c_{i2} \\ \vdots \\ C_n = \frac{1}{m} \sum_{i=1}^m c_{in} \end{cases} \quad \mathbf{Res} = \frac{1}{m} \sum_{i=1}^m \text{Res}_i \quad (3)$$

2.2.2 Bearing fault adaptive fuzzy neural network algorithm

ANFIS uses a hybrid algorithm of backpropagation and least squares to adjust the premise and conclusion parameters and can automatically generate if-then rules [26]. For a system with two inputs x and y and one output f , the corresponding T-S fuzzy inference model is first-order and has two rule sets:

Rule 1: if x is A_1 and y is B_1 , Then $f_1 = p_1x + q_1y + r_1$.

Rule 2: if x is A_2 and y is B_2 , Then $f_2 = p_2x + q_2y + r_2$.

In the formula, A_i and B_i are fuzzy sets, and $f(x, y)$ is the accuracy of the conclusion output. The ANFIS structure diagram is shown in Fig. 1.

The ANFIS is mainly composed of 5 layers, and the functions of each layer are as follows:

- (1) Layer 1: The membership function layer of the input variables, which mainly completes the fuzzification of the input variables.
- (2) Layer 2: This layer is responsible for multiplying the output functions of the different rules after fuzzification and obtaining the new output function.
- (3) Layer 3: Normalization layer for all rule strengths, normalizing different rules for different nodes.
- (4) Layer 4: Calculating the output of fuzzy rules.

Fig. 2 Bearing temperature prediction flow chart

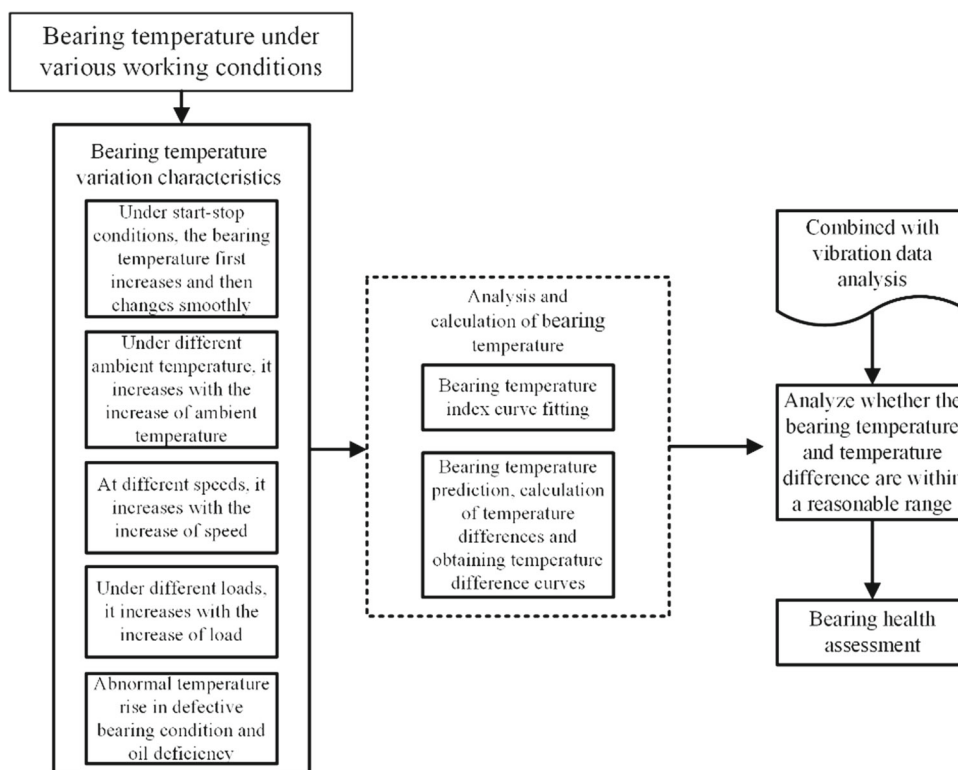
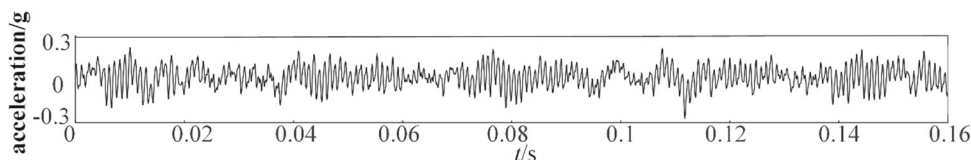


Fig. 3 Normal state time domain waveform



(5) Layer 5: Summing the output of each node to obtain the total output

2.2.3 Research on the early warning algorithm of bearing temperature trends

Temperature is the most direct indicator to measure the thermal state of the bearing. The existing temperature early warning method uses the absolute temperature threshold as the early warning standard, which can easily lead to missed and false alarms. When the threshold value is set low, it is easy to cause the phenomenon that the bearing temperature is too high to be misjudged as an abnormal state when the ambient temperature is greatly affected or the load is heavy. When the threshold value is set too high, abnormal bearing temperatures are not detected in time.

In summary, according to the abnormal operating temperature rise characteristics of bearings, using abnormal temperature rise trends different from their historical temperature rise models as a first level warning, combined with the vibration measurement data, the absolute temperature

exceeding the set threshold is used as a secondary alarm to improve the existing bearing temperature warning method. The historical operating data and real-time measurement data of the bearings at different ambient temperatures are used to identify abnormal temperature rise trends and to detect fault precursors in advance. Bearing temperature prediction ideas are shown in Fig. 2.

3 EEMD decomposition of the original vibration signal

3.1 Characteristic analysis of the vibration signal

In the experiment, vibration data were collected using the vibration module of the CWRU test bench. The bearing type selected for the experiment was the SKF 6205 deep groove type bearing, whose parameters are shown in Table 1.

The experimental data include the vibration signals collected in four bearing states: normal, bearing rolling component fault, outer ring fault and inner ring fault, at 1750 r/min, the sampling frequency of the signals is set to 12 kHz,

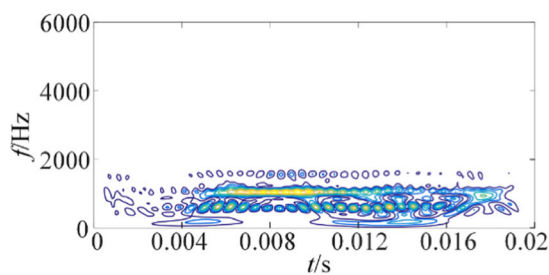
Table 1 6205 bearing specifications and dimensions

Category	Parameter	Category	Parameter
Bearing type	Deep groove ball bearing	Pitch diameter/mm	38.5
Inner ring diameter/mm	25	Number of balls	7
Outer ring diameter/mm	52	Contact angle/degree	0
Thickness/mm	15	Dynamic load/kN	14
Weight/kg	0.128	Static load/kN	7.85

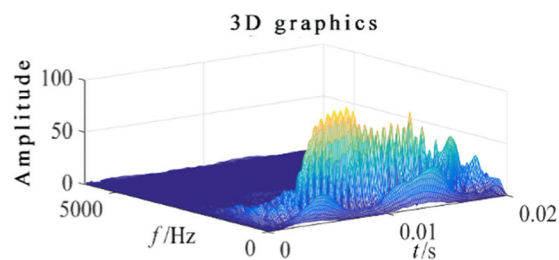
2048 time domain data are taken for each set of samples, and the vibration data within 0.02 s are taken for bispectrum transform, as shown in Figs. 3, 4, 5, 6, 7, 8, 9 and 10.

Figures 3 and 4 show that the time domain waveform of the bearing under normal conditions varies relatively smoothly without shock components. Figure 4a, b spectrograms show that the frequency components of vibration acceleration in the normal state are mostly concentrated in the low frequency band, especially between 0 and 1000 Hz with a dense distribution and large amplitude; above 2000 Hz, the frequency amplitude is almost zero, and in the high frequency band, there are only a few frequency components.

Figures 5 and 6 show that when scratches are present on the surface of the rolling body, the time domain signal produces shock vibrations with long periodic variations in the amplitude of the vibration. Figure 6a, b spectrograms show that the energy is concentrated in the middle and high frequency bands, with the 2500–3500 Hz band being the main component, and the energy amplitude produces a hump at 0.004 s and 3000 Hz, with a significant impulse component.



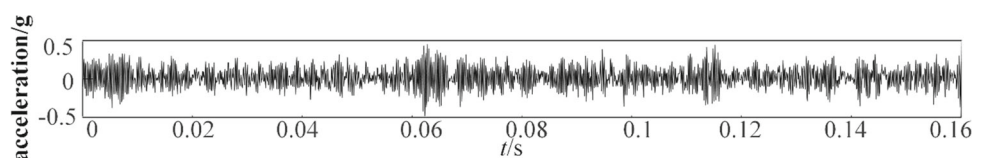
a) Normal state bispectral 2D amplitude map



b) Normal state bispectral 3D amplitude map

Fig. 4 Normal state spectrogram

Fig. 5 Bearing rolling component fault time domain waveforms



Figures 7 and 8 show that when there is damage to the inner ring of the bearing, due to the radial clearance of the bearing, the change in the low frequency band below 800 Hz is not very significant, but at 0.008 s and 0.014 s, a large number of group peaks appear in the 1800 Hz and 3600 Hz bands, i.e., the energy is basically concentrated in the middle frequency band. Figure 8a, b shows that there is a periodic variation in the amplitude of the vibration, i.e., amplitude modulation occurs.

Figure 9 shows that when there is damage to the outer ring of the bearing, the vibration signal is a series of high-frequency attenuation vibrations, and high frequencies are the main component. From the point of view of the time domain signal, the position between the damage point and the bearing direction is fixed, it is independent of the vibration modulation, and the vibration signal is pulse-modulated. Figure 10a, b shows that peaks appear in the 2000–3000 Hz band at 0.01 s and 0.02 s and that there is a periodic variation in the amplitude of the vibration.

Therefore, the vibration signal in the defective state of the bearing contains a wealth of fault precursor features, and through the vibration signal in the bearing fault state for feature extraction, it can achieve the bearing of different fault precursors and locations of discrimination.

3.2 EEMD feature extraction algorithm for vibration signals

EEMD is used to decompose the vibration signal, and all IMF components of the decomposition are used for feature component extraction. Based on this, the envelope of each order IMF component is extracted and used for feature extraction in bearing fault states. The IMF component

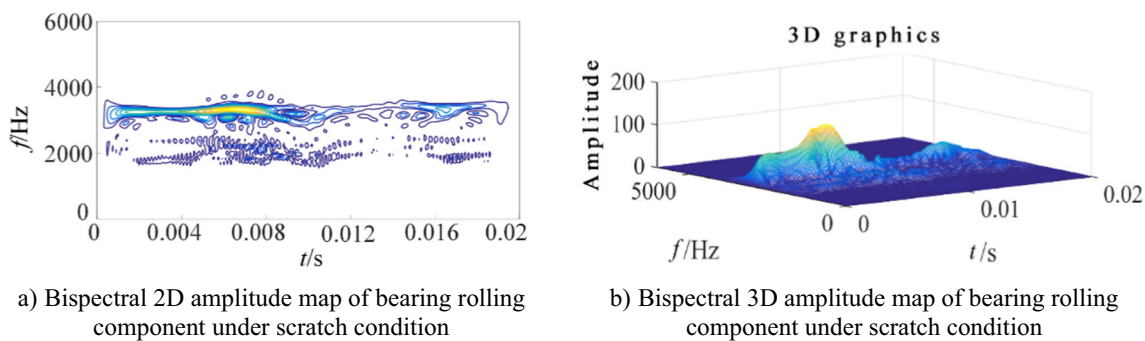


Fig. 6 Spectrograms of the bearing rolling component in the scratched state

Fig. 7 Inner ring fault time domain waveform

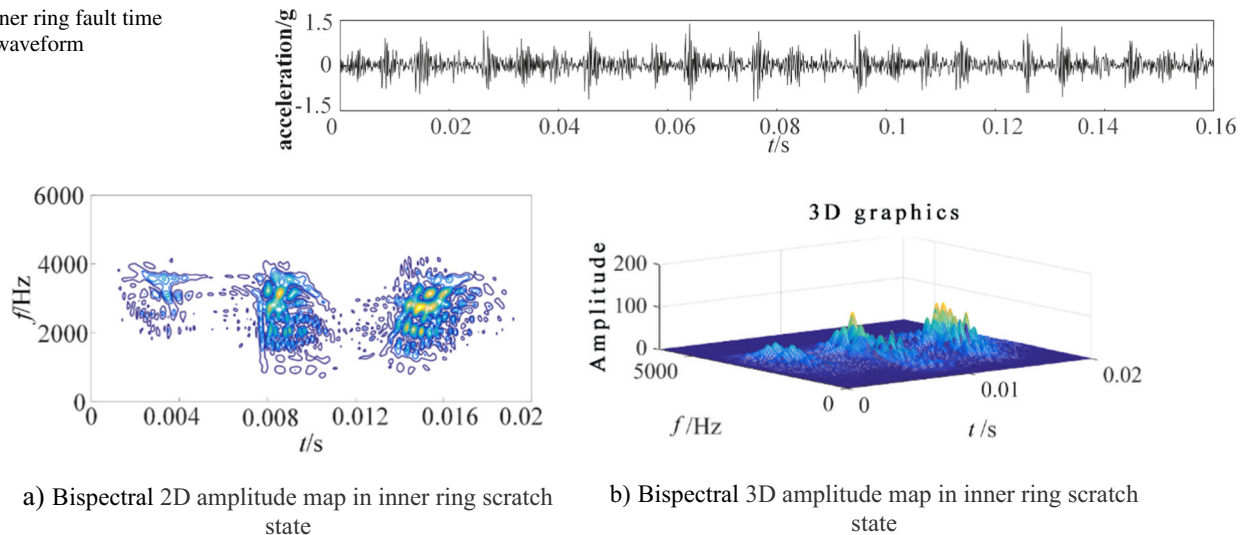


Fig. 8 Spectrogram in the scratched state of the inner ring

Fig. 9 Time domain waveforms in the outer ring scratch condition

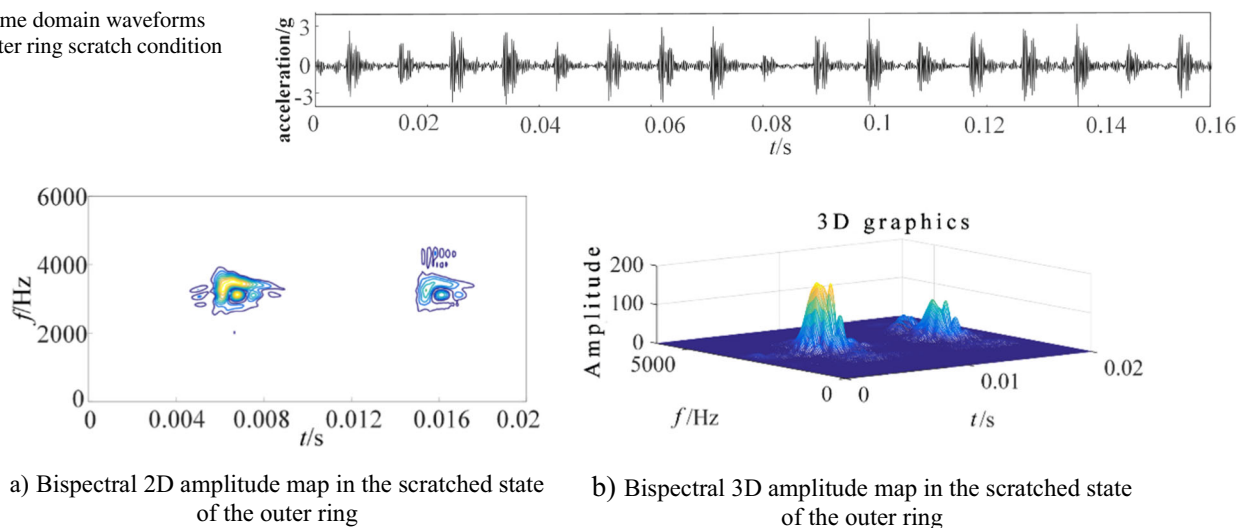


Fig. 10 Spectrogram in the scratched state of the outer ring

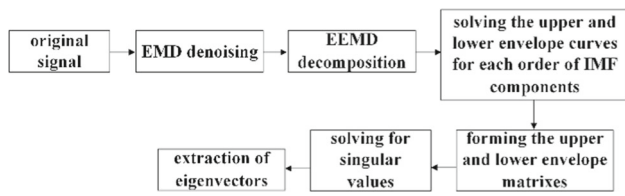


Fig. 11 Flow chart of the IMF singular value vibration-based feature extraction method

of the EEMD decomposition contains all signal characteristics in the high- and low-frequency bands, providing a more comprehensive understanding of the vibration damage characteristics in bearing fault conditions. The steps are shown in Fig. 11. The EMD hard thresholding algorithm is used first for noise reduction of vibration signals, which can improve the signal-to-noise ratio of vibration data and obtain more distinctive vibration signal characteristics. If we only rely on EEMD itself for signal noise reduction, the local variation characteristics and time-varying characteristics of the signal after processing are less effective compared with now.

3.2.1 Analysis of the EMD threshold denoising method

There is a wealth of fault information in bearing vibration signals, but the acquisition process often results in the fault characteristics being masked due to interference from external noise or other reasons, making the signal more difficult to process; therefore, noise reduction is required before the vibration signal can be analyzed. Since EMD has good local characteristics and adaptivity, it is suitable for filtering and denoising nonstationary signals, so this paper chooses EMD threshold denoising.

The basic idea of EMD threshold denoising is to decompose the original signal to obtain each order of IMF components, select a suitable threshold for each order of IMF components, and then carry out EMD reconstruction. The steps are as follows:

- (1) Vibration signal decomposition: EMD decomposition of the given signal to obtain the IMF components of each order.
- (2) Selecting the appropriate threshold: The threshold function is used to compress the IMF components of each order.

$$x_i = \sum_{i=1}^N c_i + r \tag{4}$$

In practice, the threshold is usually fixed:

$$\gamma = \sigma \sqrt{2 \ln(N)} \tag{5}$$

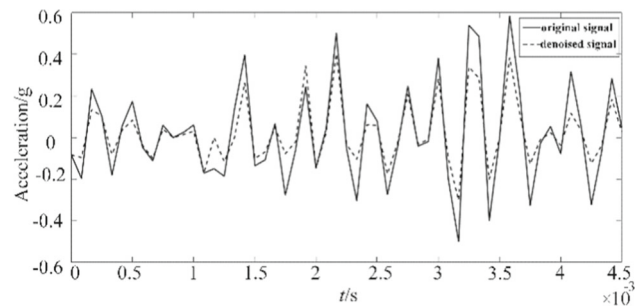


Fig. 12 Inner ring scratched vibration waveform diagram

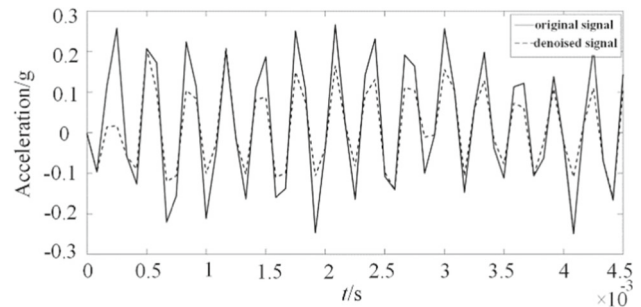


Fig. 13 Bearing rolling component scratched vibration waveform diagram

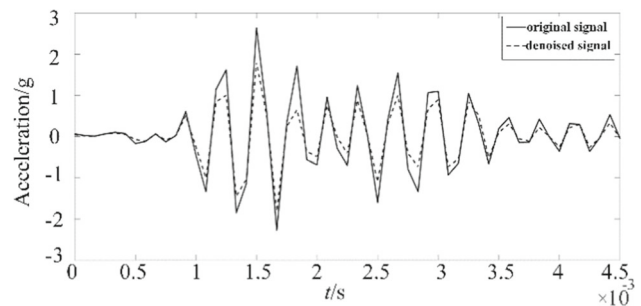


Fig. 14 Outer ring scratch vibration waveform diagram

In the formula, σ^2 is the noise variance, N is the sampling length, and γ is the fixed threshold.

- (3) Vibration signal reconstruction: signal reconstruction of the processed IMF components.

Figures 12, 13 and 14 show the waveforms of the vibration signal after denoising using the EMD hard thresholding method. The waveforms tend to flatten out after denoising, indicating that EMD threshold denoising has a certain suppression effect on the high-frequency part of the vibration signal.

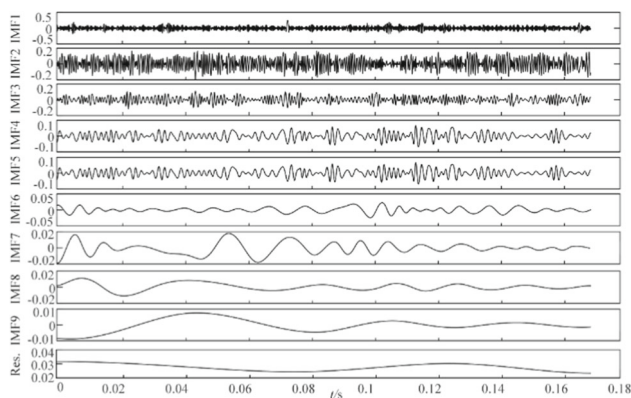


Fig. 15 EEMD decomposition diagram under normal operating conditions

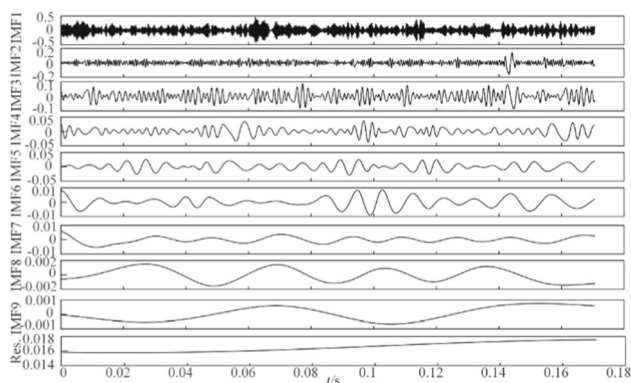


Fig. 16 EEMD decomposition of bearing rolling components in a scratched condition

3.2.2 Analysis of the method for extracting singular value features of the IMF component envelope matrix of various orders

After the vibration data have been denoised by EMD, EEMD is used to decompose the vibration signals of the motor bearing under normal and faulty operating conditions, and the results are shown in Figs. 15, 16, 17 and 18. The vibration signal is decomposed into 9 IMF components and 1 residual signal under normal conditions and 10, 9 and 9 IMF components and 1 residual signal under inner ring, outer ring and rolling body damage conditions, respectively.

After decomposing the original vibration signal by EEMD in the defective state, the upper and lower envelope curves are obtained for each order of IMF components to form the upper and lower envelope matrices, respectively, and the singular values of the two matrices are solved to extract the vibration signal eigenvalues for fault characterization. Since the singular values of the upper and lower envelope matrices obtained after the EEMD decomposition are equal, only one set of matrix singular values needs to be calculated. Finally, the

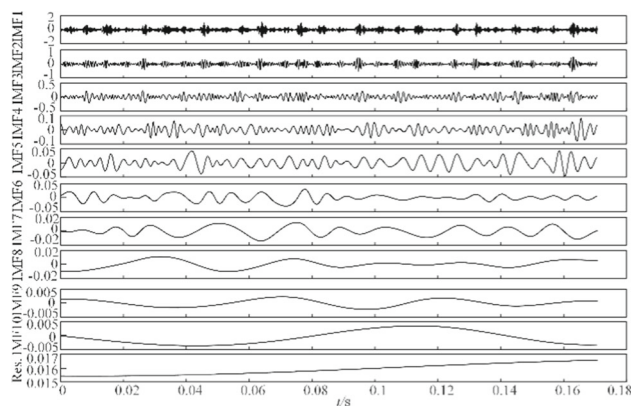


Fig. 17 EEMD decomposition of the inner ring in the scratched condition

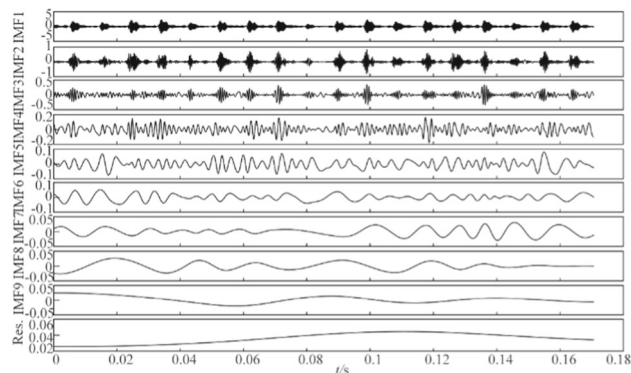


Fig. 18 EEMD decomposition of the outer ring in the scratched condition

vibration signals of different damage locations in the defective state were selected for vibration feature extraction, and some of the results are shown in Table 2.

From the analysis in Table 2, it can be seen that the method of using the singular value of the envelope can reflect the different characteristics of various bearing operating conditions. The characteristic value of the bearing under normal operation is concentrated at approximately 1.34; when the bearing rolling component faults are concentrated at approximately 3.6; when the inner ring faults are concentrated at approximately 7.2; and when the outer ring faults are set at approximately 17.8, the analysis of these results can be obtained, and the characteristic value under different failure positions is different.

To eliminate the effect of a particular IMF component of the decomposition on the results, the singular values of envelope need to be normalized, and some of the results are shown in Tables 3, 4, 5 and 6.

Table 2 Characteristic value of the vibration of the bearing under the running state (part)

State	λ_1	λ_2	λ_3	λ_4	λ_5	λ_6	λ_7	λ_8
Normal	1.341 1	0.636 9	0.392 6	0.392 6	0.366 6	0.257 5	0.023 9	0.047 3
Normal	1.379 5	0.767 5	0.641 7	0.946 0	0.594 9	0.246 7	0.125 1	0.076 1
Bearing rolling element faults	3.612 9	0.653 7	0.687 3	0.272 6	0.255 9	0.075 1	0.047 2	0.021 0
Bearing rolling element faults	3.802 3	0.650 7	0.692 4	0.253 9	0.250 2	0.055 5	0.050 1	0.019 2
Inner ring faults	7.245 7	2.995 8	1.789 6	0.533 3	0.378 0	0.256 7	0.141 8	0.125 3
Inner ring faults	7.027 8	3.093 9	1.698 3	0.846 4	0.478 2	0.260 2	0.175 1	0.091 6
Outer ring faults	17.870	3.995 0	1.648 7	1.135 6	0.650 4	0.460 6	0.369 4	0.213 3
Outer ring faults	17.147	5.422 9	1.871 2	1.272 9	0.564 3	0.497 6	0.308 2	0.263 3

Table 3 Vibration characteristic values for bearings under normal conditions

State model	Sample 1	Sample 2	Sample 3	Sample 4	Sample 5	Sample 6
Normal state envelope model	0.7618167	0.6703065	0.7747427	0.7893601	0.8096204	0.8100185
	0.3618266	0.3729537	0.3634536	0.3884159	0.3801610	0.4082248
	0.2230291	0.3118412	0.2180169	0.2069541	0.2122011	0.2219285
	0.2082369	0.2891095	0.2535997	0.2406752	0.1837573	0.1446691
	0.1462888	0.1198982	0.1194669	0.1315498	0.1404013	0.1442834
	0.0135847	0.0608172	0.0434008	0.0756838	0.0262365	0.0932289
	0.0268820	0.0369892	0.1642409	0.0238165	0.0203862	0.0151848

Table 4 Vibration characteristic values for bearing rolling components in a scratched condition

State model	Sample 1	Sample 2	Sample 3	Sample 4	Sample 5	Sample 6
Bearing rolling element scratch envelope model	0.9682116	0.9614050	0.9651020	0.9704741	0.9707225	0.9705809
	0.1730979	0.1827073	0.1811340	0.1722210	0.1645957	0.1693122
	0.1502962	0.1749073	0.1679409	0.1423785	0.1525131	0.1534141
	0.0745828	0.0877900	0.0727968	0.0605720	0.0694034	0.0543683
	0.0638118	0.0599482	0.0408592	0.0631489	0.0451208	0.0489236
	0.0145101	0.0161662	0.0195476	0.0204413	0.0180810	0.0174201
	0.0077076	0.0125307	0.0107356	0.0098212	0.0110256	0.0087726
	0.0104827	0.0025688	0.0099058	0.0087791	0.0066740	0.0063410

Table 5 Vibration characteristic values in the condition of bearing inner ring scratching

State model	Sample 1	Sample 2	Sample 3	Sample 4	Sample 5	Sample 6
Inner ring fault envelope model	0.9004087	0.9073715	0.9017338	0.9089530	0.8978364	0.9069636
	0.3540357	0.3382198	0.3450093	0.3400395	0.3718749	0.3461526
	0.2278886	0.2204955	0.2161749	0.2090517	0.2099571	0.2025235
	0.0901744	0.0959924	0.1272456	0.0999300	0.0888629	0.1123931
	0.0470121	0.0522606	0.0515471	0.0582133	0.0504356	0.0523776
	0.0355401	0.0345454	0.0361953	0.0253408	0.0265076	0.0294639
	0.0123188	0.0204267	0.0281486	0.0141215	0.0104427	0.0175134
	0.0152666	0.0104656	0.0127250	0.0160761	0.0162678	0.0053857

Table 6 Vibration characteristic values in the condition of bearing outer ring scratching

State model	Sample 1	Sample 2	Sample 3	Sample 4	Sample 5	Sample 6
Outer ring fault envelope model	0.9523427	0.9898410	0.9689637	0.9449475	0.9879939	0.9285249
	0.2747596	0.1015809	0.2166179	0.2988357	0.1291828	0.3466933
	0.1050965	0.0809779	0.0893981	0.1031153	0.0651456	0.1056922
	0.0629944	0.0441212	0.0615744	0.0701444	0.0424595	0.0664157
	0.0360330	0.0281255	0.0352664	0.0310994	0.0254337	0.0314090
	0.0266272	0.0181463	0.0249745	0.0274206	0.0174805	0.0252118
	0.0165830	0.0111745	0.0200318	0.0169881	0.0112268	0.0146265
	0.2747596	0.1015809	0.2166179	0.2988357	0.1291828	0.3466933

4 Diagnostic analysis of bearing vibration and temperature faults

4.1 Analysis of bearing vibration fault diagnosis

If the singular values of the vibration data from the EEMD decomposition are used directly as input to the ANFIS model, the model will have too many dimensions and take too long to train. Therefore, the dimensionality of the vibration eigenvalue data needs to be reduced by introducing the PCA algorithm to improve the training speed and accuracy of the model [27].

4.1.1 Vibration eigenvalue PCA dimension reduction

PCA is a linear dimension reduction technique where the eigenvectors are obtained by taking the covariance matrix of the sample matrix and forming the transformation matrix. The steps of the PCA algorithm are as follows:

- (1) If the original data X contains n samples and each sample has m variables, unitary transformation is performed on the $m \times n$ order sample matrix to obtain the normalized matrix U .

$u_{ij} = (x_{ij} - \bar{x}_j) / s_j$ $i = 1, 2, \dots, m; j = 1, 2, \dots, n$ (1) in the formula:

$$\bar{x}_j = \sum_{i=1}^n x_{ij} / n; s_j^2 = \sum_{i=1}^n (x_{ij} - \bar{x}_j)^2 / (n - 1).$$

- (2) Calculate the correlation coefficient of the matrix U :

$$R = U^T U / (n - 1) \tag{6}$$

- (3) Solve for the characteristic roots of the matrix R and its eigenvectors to obtain the m characteristic roots and eigenvectors of the matrix R . Calculate the number of

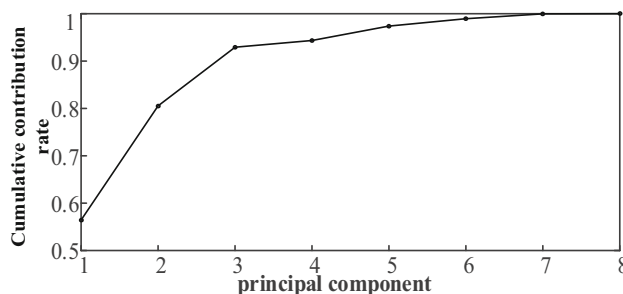


Fig. 19 Cumulative contribution rate of sample characteristics

principal components p , and obtain its eigenvector b_j .

$$|R - \lambda E| = 0 \tag{7}$$

- (4) Combine the standardized indicator variables into the principal component Z :

$$Z = \{z_1, z_2, \dots, z_p\} \tag{8}$$

in the formula: $z_j = u_i^T b_j, j = 1, 2, \dots, p$.

- (5) Weighted summation of p components and evaluation.

The 220 groups of sample vibration eigenvalue data were subjected to PCA to form a 220×8 order numerical matrix, and the PCA dimension reduction process was carried out using the princomp function in MATLAB. The results are shown in Fig. 19. Figure 20 shows that the cumulative contribution of the first principal component of X amounted to 56.44%, and the cumulative contribution of successive to the fifth principal component reached 97.37%. To increase the accuracy of the bearing fault diagnosis, the data are converted from 8 to 5 dimensions for subsequent ANFIS training.

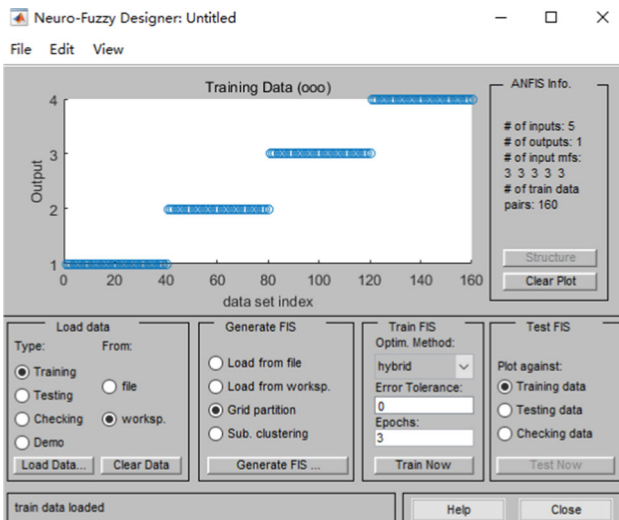


Fig. 20 ANFIS training model

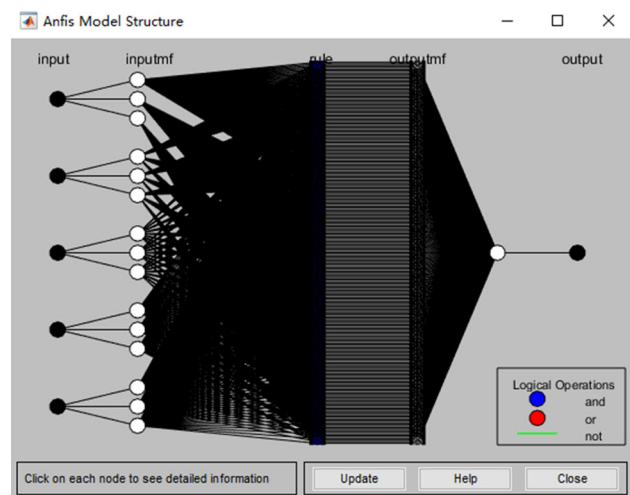


Fig. 21 ANFIS structure diagram

4.1.2 Vibration characteristics ANFIS fault diagnosis analysis

Forty samples are randomly selected for each condition as training samples for the ANFIS, the singular values of the envelope matrix of the vibration signals in the 4 states of the bearing are calculated, and the first 5th order IMF components are selected as the eigenvectors of the ANFIS model, for a total of 160 sets of training sample data. The ANFIS training model is shown in Fig. 20.

Then, 15 samples under each working condition were randomly selected, a total of 60 groups of test samples, and the respective feature vectors were obtained according to the above method, which were input into the ANFIS model for testing, and the corresponding running state of bearings was taken as its expected output. As the above samples of collected bearing runs correspond to four states, this paper selects 4 nodes for the output of the ANFIS model, where output {1} indicates the normal operating condition of the bearing, output {2} indicates the fault operating condition of the inner ring scratch damage, output {3} indicates the fault operating condition of the outer ring scratch damage, output {4} the fault operating condition of the rolling element scratch damage of the bearing, i.e., Five input nodes and 4 output nodes corresponding to the ANFIS model. In the bearing fault diagnosis model, the allowable error is set to 0, and 3 membership functions are set for each input quantity, as shown in Fig. 21.

The model is determined according to the ANFIS network design principles in the previous section, the training function is selected as the Gaussian-type Gaussmf algorithm, and the time of training was 50. After training, 60 sets of test samples are input, and the output is obtained. The training error curve is shown in Fig. 22. The training error curve is shown in

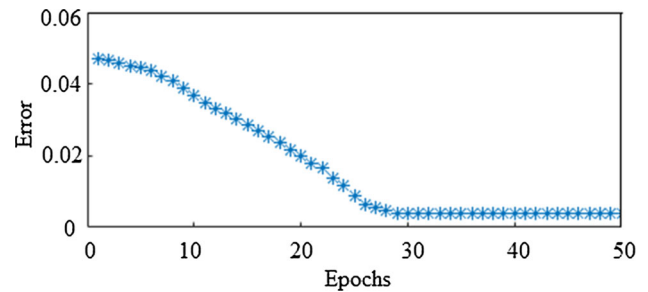


Fig. 22 ANFIS error curve

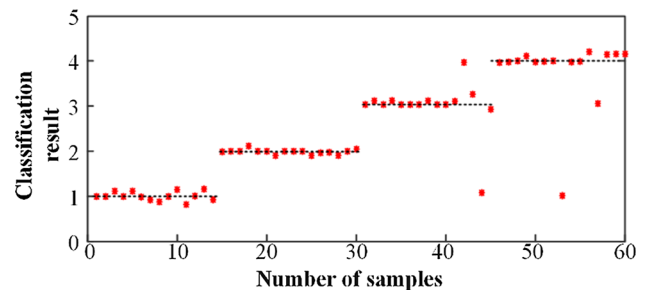


Fig. 23 ANFIS simulation classification result diagram

Fig. 22, where the network training error converges to 0.003 945 6 at 32 training times.

After the ANFIS training was completed, the results are shown in Fig. 23. Among them, one of the outer ring scratch fault samples is identified as the normal state, and the other sample is identified as the bearing rolling components scratch state. One of the bearing rolling component scratch samples was identified as the outer ring scratch condition, and one was identified as the normal condition. Among the 60 sets of test samples, 4 sample points were incorrectly diagnosed, and the overall classification rate reached 93.3%, proving

Table 7 Fault diagnosis comparison result

Fault diagnosis method	Number of training samples	Number of test samples	Number of correct diagnoses	Correct rate
BP neural network	160	60	53	88.3%
PCA-ANFIS	160	60	56	93.3%



Fig. 24 7005c bearing

that the method in this paper is an effective way to diagnose the condition of bearings.

To test the application effect of PCA-ANFIS, the BP (back propagation) neural network without PCA treatment was chosen for comparison analysis. In this paper, a three-layer neural network with 10 neurons in the hidden layer is established, in which the input layer corresponds to 8 eigenvalues of each order of IMF components and the output layer corresponds to 4 operating states of the bearings, and the results are shown in Table 7. As seen from Table 7, when using the BP neural network for diagnosis, a total of 53 samples were correctly diagnosed out of 60 groups of test samples, with a correct diagnosis rate of 88.3%. The results show that the PCA-ANFIS model is more accurate than the BP neural network.

4.2 Diagnosis method of abnormal temperature rise of bearings

From the above analysis, it can be seen that when using only bearing vibration detection, there are errors in the state identification, which cannot fully reflect the bearing state, especially when the bearing is out of oil or low on oil, and

the ideal effect cannot be achieved. Therefore, this paper proposes a combined temperature and vibration early warning method, using vibration signal detection to react to bearing parts that wear serious faults; when the bearing is out of oil or low oil, using a combination of temperature and vibration early warning methods, to achieve the purpose of comprehensive detection of the current operating status of the bearing.

The motorized spindle 7005C bearing data were used for verification, the 7005C bearing is shown in Fig. 24, and the 7005C bearing parameters are shown in Table 8.

4.2.1 Analysis of bearing temperature rise under normal conditions

When the motor is started normally, the temperature of the outer ring of the bearing rises rapidly and stabilizes around a fixed value. To ensure the validity of the temperature data, the temperature rise curves of bearings under the same working conditions were recorded under five start-up conditions, with room temperature at 22°C and speed at 10,000 r/min, as shown in Fig. 24. It can be seen that the temperature rise of the bearing reaches a stable state after 20 min of operation, and the temperature value of the outer ring of the bearing is stable at approximately 35 °C, so 35 °C is chosen as the comparison temperature of the bearing under the state of lack of oil or less oil.

Based on a practical engineering background, this paper considers the influence of the rotating speed on the bearing temperature rise. First, the motor load is fixed, the temperature rise of the outer ring of the bearing is recorded at different speeds of the motor, and the temperature rise value is corrected according to the speed to improve the accuracy of the bearing temperature rise warning. Figure 25 shows the average curve of the absolute temperature of the outer ring of the bearing at different speeds. It can be seen that, under the same working conditions, the value of the temperature of the

Table 8 Specifications for 7005C

Category	Parameter	Category	Parameter
Bearing type	Angle contact ball bearing	Pitch diameter/mm	36
Inner ring diameter/mm	25	Number of balls/pieces	13
Outer ring diameter/mm	47	Contact angle/degree	15
Thickness/mm	12	Dynamic load/kN	12.3
Weight/kg	0.182	Static load/kN	8

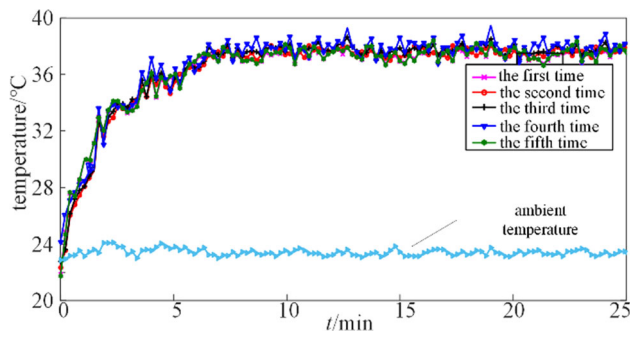


Fig. 25 Temperature rise curve under the starting condition of bearing

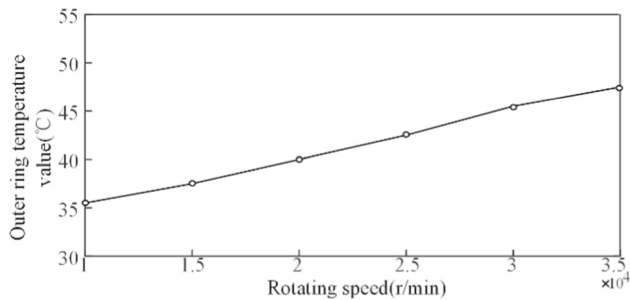


Fig. 26 Absolute temperature curve of the bearing outer ring at different speeds

outer ring of the bearing increases with the increase of the speed of the bearing.

4.2.2 Characteristic analysis of bearing failures in the oil deficiency condition

Bearing vibration and outer ring temperature data were collected in the oil deficiency condition at a speed of 10,020 r/min, room temperature of 22 °C and fixed load. From the calculations, the theoretical characteristic frequency of the bearing at 10,020 r/min is 165 Hz. The EEMD decomposition of the vibration signal at 140 h of operation of the bearing in the oil-deficient condition and the envelope spectrum analysis of its first three orders of IMF components are carried out to extract the characteristic frequencies to obtain Fig. 26.

Figure 26 shows that the point with the largest amplitude of the envelope spectrogram of the first three orders of IMF components corresponds to a frequency of 163.1 Hz, which is less different from the inherent vibration frequency of the spindle and can be considered to have no fault frequency occurrence. 489.4 Hz is close to the frequency components of the inherent frequency of the bearing, i.e., the frequency components with the largest amplitude are caused by the spindle vibration. If analyzed according to the vibration characteristics, the result is normal operation of the bearing. This clearly does not correspond to the actual situation, so it can be concluded that a single vibration signal component cannot

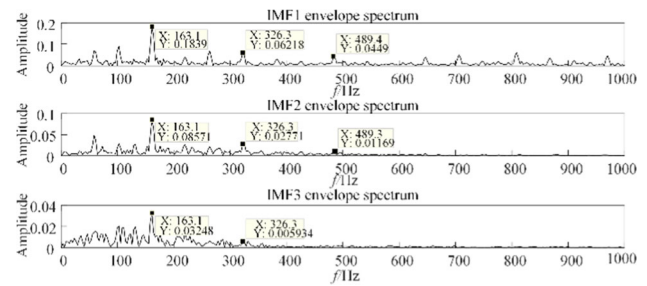


Fig. 27 The first three orders of the IMF component envelope of the signal in the oil deficiency condition

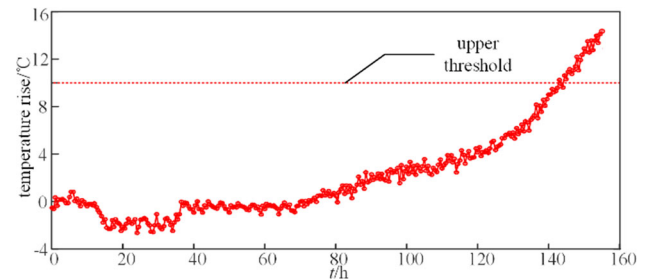


Fig. 28 Temperature rise curve of the bearing outer ring

accurately diagnose the state of the bearing. To achieve an accurate diagnosis of the bearing oil deficiency, it is necessary to combine the temperature characteristics to diagnose it, and the temperature rise of the outer ring of the bearing under oil deficiency is shown in Fig. 27.

The experimental bearing speed is set to 10,020 r/min, the room temperature is 22 °C, the absolute bearing temperature value under normal conditions is 36 °C, and the preset temperature confidence interval for healthy operation of the motor bearing is [10, 10] °C. As seen from Fig. 28, the temperature rise of the bearing under the state of oil deficiency does not change much at the beginning. At this time, the bearing wear degree is small, and the temperature rise is slightly reduced. After 80 h of operation, the bearing temperature rises rapidly, and after 145 h, the outer ring temperature value of the bearing exceeds the upper limit of the bearing temperature rise threshold, reaching the bearing temperature rise alarm state. Therefore, the temperature rise of the outer ring of the bearing under the state of oil deficiency can be used to achieve the purpose of early warning.

In the defective state, the vibration signal for EEMD decomposition, combined with the PCA-ANFIS fault diagnosis model, can be the bearing normal state and fault state accurate classification to achieve the bearing state diagnosis. In the state of oil deficiency, the bearing vibration signal and temperature rise trend need to be combined to detect the fault characteristics and issue a warning signal, providing a reliable guarantee for the safe and stable operation of the motor bearing.

5 Conclusion

This paper conducts a study on the early warning method of bearing health diagnosis and establishes a secondary warning model based on the EEMD-PCA-ANFIS vibration analysis model and bearing temperature rise trend. Through the research done in this paper, the following conclusions are obtained:

- (1) The EEMD-PCA-ANFIS vibration signal bearing fault diagnosis model was established, and the EMD hard threshold method was used to reduce the noise of the original vibration data, which improved the signal-to-noise ratio of the vibration data. The PCA algorithm was introduced into the vibration signal feature extraction, and through PCA dimensionality reduction, the proportion of IMF pseudo components that existed was reduced, and a set of optimal vibration feature input parameters was obtained, which better solved the ANFIS classification model with too many dimensions. The results show that the vibration model based on EEMD-PCA-ANFIS can accurately diagnose the normal state, inner ring damage state, outer ring damage state and rolling body damage state of the bearing, and the correct rate reaches 93.3%.
- (2) A diagnostic model for the oil deficiency condition of bearings based on the joint analysis of vibration and temperature rise trends was designed. The results show that there is no obvious vibration shock component in the bearing in the state of oil deficiency, but the temperature rise shows an obvious rising trend, using the joint analysis model of vibration and temperature rise trend can distinguish the bearing oil deficiency state from the normal operation state and fault state, which improves the accuracy of the comprehensive warning of the bearing.

The method of bearing fault warning based on vibration signals and temperature rise trends proposed in this paper is not only applicable to general motor bearings but can also be applied to other rotating machinery and equipment, which improves the accuracy of bearing operation monitoring and fault warning and lays the foundation for the realization of intelligent fault warning algorithms with multi-information fusion.

The method proposed in this paper has limitations in the following aspects.

- (1) EEMD can effectively suppress modal confusion, but when the amount of analysis data is particularly large, the EEMD decomposition time is long and the diagnostic timeliness is poor. If the EEMD algorithm is

improved, the efficiency of the diagnosis of bearing faults can be improved.

- (2) This paper analyzes and diagnoses single-point faults of motor bearings without studying compound faults, while under actual working conditions, bearings generally exhibit multiple fault characteristics instead of a single mode. Therefore, incorporating the composite diagnosis technology of multiple faults into the fault diagnosis of motor bearings is one of the key contents to be studied in the future.

Author contributions All authors contributed to the study conception and design. Material preparation, data collection and analysis were performed by FZ, YW, SJ and TH. The first draft of the manuscript was written by YW and all authors commented on previous versions of the manuscript. All authors read and approved the final manuscript. Conceptualization: FZ; Methodology: TH; Writing—original draft preparation: YW; Writing—review and editing: FZ; Resources: SJ; Supervision: FZ.

Funding The authors did not receive support from any organization for the submitted work. The authors have no relevant financial or non-financial interests to disclose.

Declarations

Conflict of interest All authors declare that: (i) no support, financial or otherwise, has been received from any organization that may have an interest in the submitted work; and (ii) there are no other relationships or activities that could appear to have influenced the submitted work.

References

1. Qu J, Yu L, Yuan T, Tian Y, Gao F (2018) Adaptive fault diagnosis algorithm for rolling bearings based on one-dimensional convolutional neural network. *Chin J Sci Ins* 39(7):134–143
2. Shao H, Jiang H, Lin Y, Li X (2018) A novel method for intelligent fault diagnosis of rolling bearings using ensemble deep auto-encoders. *Mech Syst Signal Proc* 102:278–297
3. Zhao G, Pan B, Li F (2008) Application of condition monitoring technology in the diagnosis of bearing faults in high-speed rotating equipment [J]. *Plant Maint Eng* 12:42–43
4. Chen J, Zhang W, Luo M, Wang H (2021) Research on temperature monitoring system of inner ring of intelligent rolling bearing [J]. *Ins Tech Sens* 10:103–108
5. Gopalakrishna GK, Padubidre SP (2019) Development of low cost system for condition monitoring of rolling element bearing using MEMS based accelerometer[C]//EMERGING TRENDS IN MECHANICAL ENGINEERING 2018
6. Chen Y, Li Y, An W, Liu H, Jiang T (2021) Rolling bearing performance degradation prediction based on FBG signal[J]. *IEEE Sens J* 21(21):24134–24141
7. Tritschler N, Dugenske A, Kurfess T (2021) An automated edge computing-based condition health monitoring system: with an application on rolling element bearings[J]. *J Manuf Sci Eng* 143(7):1–10
8. Ren D, Zhang Y, Zhang W, Zhao G (2015) Embedded intelligent sliding bearing research [J]. *Light Industry Mach* 33(06):88–91

9. Zhang N, Wang N, Zhang X, Jing M (2021) Research on influence of grooving parameters on intelligent water-lubricated bearing embedded in thin film sensors. In: International Conference on Sensors and Instruments (ICSI 2021) (Vol. 11887, pp. 53-59). SPIE
10. Brusa E, Vedova MD, Giorio L, Maggiore P (2021) Thermal condition monitoring of large smart bearing through fiber optic sensors. *Mech Adv Mater Struct* 28(11):1187–1193. <https://doi.org/10.1080/15376494.2019.1655611>
11. Liu Q, Huang J (2015) A surface micromachined MEMS temperature sensor [J]. *Chin J Sens Actuators* 03:325–329
12. Zx A, Yu W A, Rw A, et al (2021) A high-speed and long-life triboelectric sensor with charge supplement for monitoring the speed and skidding of rolling bearing
13. Tao H, Wang P, Chen Y, et al (2020) An unsupervised fault diagnosis method for rolling bearing using STFT and generative neural networks[J]. *Journal of the Franklin Institute* 357(11).
14. Toma RN, Kim JM (2020) Bearing fault classification of induction motors using discrete wavelet transform and ensemble machine learning algorithms[J]. *Appl Sci* 10(15):5251
15. Niu Y, Fei J, Li Y et al (2020) A novel fault diagnosis method based on EMD, cyclostationary, SK and TPTSR[J]. *J Mech Sci Technol* 34(5):1925–1935
16. Huang Y, Luo W, Zhang R (2019) Application of improved Naive Bayes algorithm in text classification [J]. *Technol Innov Appl* 05:24–27
17. Rui ME, Hacker T, Rong C (2013) Competitive K-means, a new accurate and distributed K-means algorithm for Large Datasets[C]. In: IEEE International Conference on Cloud Computing Technology and Science, Bristol pp 17–24
18. Ling H, Qian C, Kang W, Liang C, Chen H (2019) Combination of support vector machine and K-fold cross validation to predict compressive strength of concrete in marine environment. *Construc Build Mater* 206:355–363
19. Zhiyi H, Haidong S, Lin J, Junsheng C, Yu Y (2020) Transfer fault diagnosis of bearing installed in different machines using enhanced deep auto-encoder. *Measurement* 152:107393
20. Yang J, Zhao M (2012) Fault diagnosis of traction motor bearings using modified bispectrum and empirical mode decomposition [J]. *Proceed CSEE* 32(18):116–122
21. Zhou F, Lü J, Li L, Liu J (2017) Design of intelligent fault diagnosis and early warning system of motors [J]. *Inf Control* 46(06):738–745
22. Wang X, Lu S, Huang W, et al (2021) Efficient data reduction at the edge of industrial internet of things for PMSM bearing fault diagnosis[J]. *IEEE Transactions on Instrumentation and Measurement* 99:1–1.
23. Kabul A, Unsal A (2021) An alternative approach for the detection of broken rotor bars and bearing faults of induction motor based on vibration signals[C]//2021. In: 8th International Conference on Electrical and Electronics Engineering (ICEEE)
24. Wu D, Jia Q, Yang Q, et al (2016) Fault diagnosis based on EEMD-KPCA-IGSABP for motor bearing[C]. Chinese Control Conference, Chengdu pp 6605–6610.
25. M Yabin, C Chen, S Qiqi, et al (2018) Fault Diagnosis of rolling bearing based on EMD Combined with HHT envelope and wavelet spectrum transform[C]. IEEE Data Driven Control and Learning Systems Conference, Enshi pp 481–485.
26. Jang JSR (1993) ANFIS: adaptive-network-based fuzzy inference system [J]. *IEEE Trans Syst Man Cybern* 23(3):665–685
27. Andrew KS, Jardine DL, Banjevic D (2006) A review on machinery diagnostics and prognostics implementing condition based maintenance [J]. *Mech Syst Signal Process* 20:1483–1510

Publisher's Note Springer Nature remains neutral with regard to jurisdictional claims in published maps and institutional affiliations.

Springer Nature or its licensor (e.g. a society or other partner) holds exclusive rights to this article under a publishing agreement with the author(s) or other rightsholder(s); author self-archiving of the accepted manuscript version of this article is solely governed by the terms of such publishing agreement and applicable law.